Inorganic Chemistry

pubs.acs.org/IC Article

Electrochemical Flux Synthesis of Type-I Na₈Si₄₆ Clathrates: Particle Size Control Using a Solid or Molten Na—Sn Mass Transport Mediator

Andrew Dopilka, Svilen Bobev, and Candace K. Chan*



Cite This: Inorg. Chem. 2023, 62, 565-573



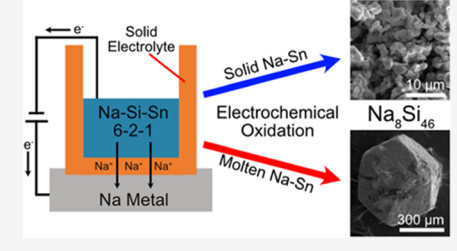
ACCESS I

Metrics & More

Article Recommendations

Supporting Information

ABSTRACT: Sodium-filled silicon clathrates have a host of interesting properties for thermoelectric, photovoltaic, and battery applications. However, the metastability of the clathrates has made it difficult to synthesize them with the desired morphology and crystallite size. Herein, we demonstrate an electrochemical method whereby Na₄Si₄ dissolved in a Sn-based flux is converted to the Na₈Si₄₆ type-I clathrate using galvanostatic (constant current) oxidation. The temperature has a large influence on the products, with the reactions at 485 °C resulting in clathrates with small particle sizes $(1-2 \ \mu\text{m})$, while larger single crystals are obtained at 538 °C. The difference in microstructure is attributed to the solid vs liquid state of the Na–Sn phase at the



reaction temperature, which is supported by the observed voltage profiles. The demonstrated method is promising for the tunable growth of Si clathrates and could be applicable to a broad range of intermetallic compounds.

1. INTRODUCTION

Sodium-filled silicon clathrates (Na-Si clathrates) are hostguest structures comprising a Si framework with Na guest atoms and have been investigated as thermoelectric, photovoltaic, 2-6 and Li-ion battery materials 7-10 with interesting properties. The metastable nature of the structures, however, requires reaction pathways that start with a high-energy precursor. The majority of reported syntheses for the type-I (Na₈Si₄₆) and type-II (Na_xSi₁₃₆, 0 < x < 24) Na–Si clathrates involve removal of Na from the Zintl phase Na₄Si₄. ^{2,10-19} The process by which this occurs has been studied before, with most successful results achieved through various oxidation methods, including thermal evaporation under vacuum^{2,11-13,17,20} or use of chemical oxidants. 19,21 Recently, it was demonstrated that electrochemical oxidation of Zintl phase precursors can be utilized to form clathrates through desodiation processes that are analogous to the reactions that rely on Na evaporation. 10,22,23 Electrochemical methods have the advantage of more control over the reaction kinetics (i.e., through modulation of the current) and the ability to observe the electrode potential in situ, which can be helpful for understanding the reaction mechanisms. For instance, while the Na evaporation rate from Na₄Si₄ in the conventional synthesis method is closely tied to the temperature of the reaction, an electrochemical cell decouples these variables, which can result in a wider range of possible reaction conditions. Our team has used such electrochemical techniques to demonstrate the synthesis of type-I silicon clathrates and type-II germanium and alloyed silicon/ germanium clathrates from the respective Zintl phase precursors in cells containing Na β'' -alumina as a solid

electrolyte. ^{10,23} In those studies, the Zintl phase precursors were prepared as pellets and pressed against the solid electrolyte. Due to the nature of the solid-state conversion reaction, the resulting clathrate products are polycrystalline and made of particles typically on the order of a few microns or smaller in size.

Recently, flux-based methods have been reported for the growth of large crystals (1–5 mm in size) of Na–Si clathrates ^{16,18,24} and other ternary²⁵ and quaternery²⁶ clathrates. For example, Morito et al. showed that subjecting a Na–Si–Sn solution (6:2:1 molar ratio) to a thermal gradient for 48 h at 500 °C resulted in evaporation of approximately 42% of the starting Na, leading to supersaturation conditions and growth of Na₈Si₄₆ single crystals with sizes in the range of 1–2 mm.¹⁸ When the heating time was increased to 72 h, about 53% of the Na had evaporated and the resulting product comprised large crystals (5 mm) of type-I and type-II Na–Si clathrates. In these flux-based methods, the growth of the Na–Si clathrates is driven by the removal of Na from the Na–Si–Sn mixture, while the Na–Sn liquid phase facilitates the diffusion of Si to enable large single-crystal growth.

To further apply the use of electrochemical methods to the controlled growth of Na-Si clathrates, the work described herein investigates the use of Na removal, via electrochemical

Received: October 29, 2022 Published: December 22, 2022





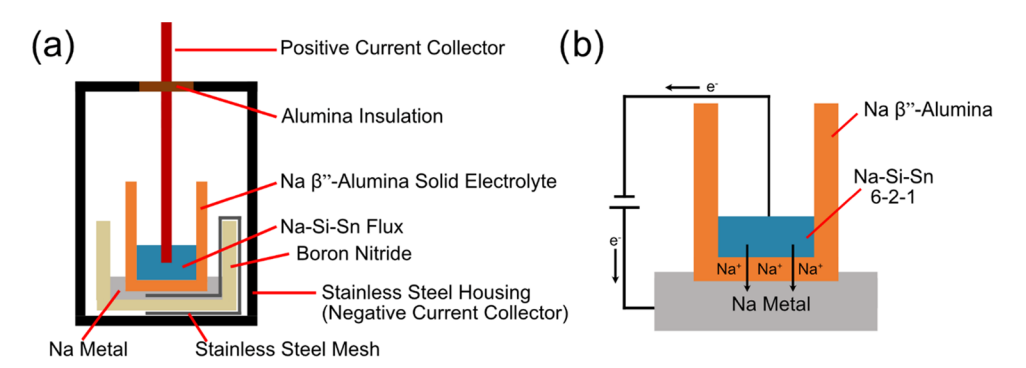


Figure 1. (a) Schematic of the two-electrode cell used for flux-mediated electrochemical synthesis of Na_8Si_{46} . A Na β'' -alumina solid electrolyte separates molten sodium (serving as counter/reference electrode) and Na-Si-Sn flux (connected to the working electrode). (b) Schematic of the electrochemically active interfaces showing the movement of Na ions and electrons.

oxidation rather than thermal evaporation, from a starting mixture of Na–Si–Sn (6:2:1) to perform reactions analogous to the flux reactions described by Morito et al. ¹⁸ In this proof-of-concept study, the two-electrode cell was modified from our previous design ¹⁰ and a cup-shaped Na β "-alumina solid electrolyte was used to separate two reservoirs of molten components, one containing molten Na metal (negative electrode, serves as both the counter and reference electrodes) and the other a Na–Si–Sn flux (positive electrode, held inside the cup and made in contact with the stainless steel current collector). A schematic of the cell configuration is presented in Figure 1a. Such a design is analogous to that in a high-temperature sodium–sulfur (Na–S) battery, wherein Na β "-alumina separates reservoirs of molten Na (negative electrode) and S (positive electrode). ²⁷

The proposed reactions for the electrochemical synthesis of Na_8Si_{46} type-I clathrate are written as follows:

Working electrode (oxidation)

$$\left(\frac{23}{2}\right)$$
Na₄Si₄ $\rightarrow 38$ Na⁺ + 38 e⁻ + Na₈Si₄₆

Counter electrode (reduction):

$$Na^+ + e^- \rightarrow Na$$

Overall reaction:

$$\left(\frac{23}{2}\right)$$
Na₄Si₄ $\to 38$ Na + Na₈Si₄₆

We find that this new, flux-mediated electrochemical approach is effective for the preparation of $\mathrm{Na_8Si_{46}}$ clathrates with different microstructures depending on the reaction conditions, with the temperature and ability of mass transport of Si through the Na–Sn phase playing an important role on the clathrate particle size.

2. EXPERIMENTAL SECTION

The preparation of the Na₄Si₄ Zintl phase precursor was conducted as reported previously^{9,10} (see the Supporting Information) and the phase was confirmed using powder X-ray diffraction (PXRD) (Figure S1). The flux synthesis was carried out in a custom-made reactor shown schematically in Figure 1a with photographs and additional description in Figure S2 and the Supporting Information. The reactor was sealed and heated in a muffle furnace inside an Ar-filled glovebox. When the furnace was set to 500 and 550 °C, the temperature measured inside was 485 and 538 °C, respectively (see the Supporting Information). After the reactor reached the desired temperature, an anodic constant current was applied to the working electrode, causing

the movement of Na $^+$ ions from the Na–Si–Sn mixture through the Na β'' -alumina electrolyte into the reservoir of molten Na metal (Figure 1b). The electrochemical reactions were carried out using the galvanostatic intermittent titration technique (GITT), which involves current pulses followed by rest periods at open circuit. ²⁸ Details of the current and relaxation times can be found in the voltage profile captions. The reaction was performed with different flux compositions, current densities, and reaction temperatures to elucidate the product formation mechanisms. After the synthesis, the products were washed with alcohol to remove Na and hydrochloric acid to remove Sn following previously reported procedures. ^{25,26} The recovered powders were characterized with powder X-ray diffraction (PXRD), scanning electron microscopy (SEM) with energy-dispersive X-ray spectroscopy (EDS), and single-crystal X-ray diffraction (SCXRD).

3. RESULTS AND DISCUSSION

The GITT method was used to carry out the electrochemical synthesis of $\mathrm{Na_8Si_{46}}$ to allow for observation of the quasi-equilibrium potential of the cell without contributions from kinetic effects or internal cell resistances. As Na is removed from the reservoir containing the Na–Si–Sn flux, the potential increases and the voltage profile will exhibit plateaus and sloped regions that coincide with different processes in the reaction. However, the voltage measured while current is applied can be affected by internal resistances and polarizations, making it larger than the voltage measured after relaxation. In the subsequent discussion of the results, we hence consider the reaction mechanisms by referring to the open-circuit potential (OCP) measured at the end of each relaxation step.

First, control experiments were performed where the flux was prepared without Na₄Si₄ (i.e., containing no precursor for the clathrate) to evaluate the cell voltage vs flux composition in the absence of clathrate formation. On the basis that Morito et al. showed clathrate synthesis was possible in a Na-Si-Sn flux at 500 °C, 18 we chose a similar reaction temperature for our reactions. Figure 2a shows the GITT voltage profiles obtained at a reaction temperature of 485 °C with a flux starting composition of Na₄Sn. The initial OCP was around 25 mV vs Na/Na⁺, which is very close to the voltages of 22-24 mV measured for a liquid Na-Sn alloy containing 80 atom % Na over a temperature range of 435–625 °C.²⁹ Upon applying a constant current density of 1.91 mA/cm², the voltage continuously increased as the amount of Na in the flux decreased. When the OCP reached 40 mV, the voltage remained constant as Na was removed until the flux reached a composition of around Na₂Sn. Further desodiation of the flux resulted in an increase in the potential until a larger plateau at

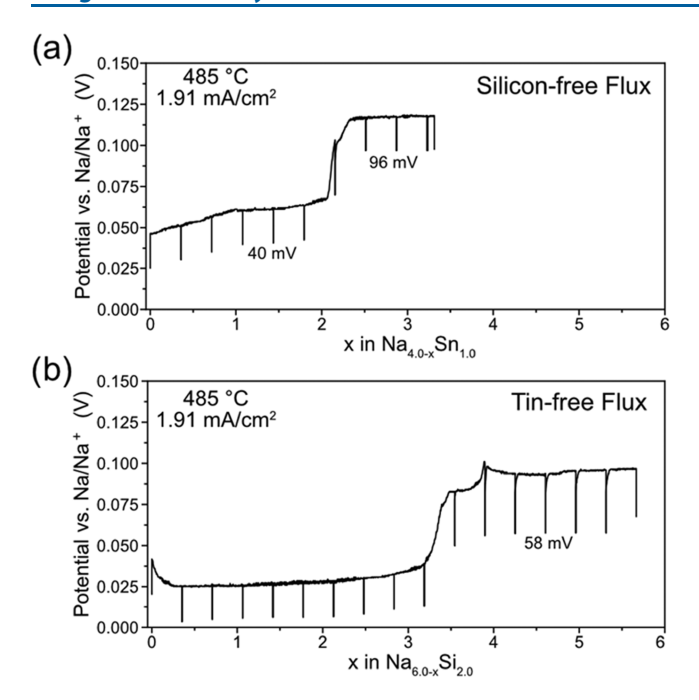


Figure 2. Galvanostatic intermittent titration technique (GITT) voltage profile at 485 $^{\circ}$ C (2 h pulses at 1.91 mA/cm² separated by 10 min of relaxation at OCP) for desodiation of (a) Na₄Sn and (b) Na₆Si₂.

96 mV was observed. The reaction was stopped once the flux composition was approximately $Na_{0.7}Sn$ (calculated from the amount of charge passed through the electrochemical cell during the GITT).

Next, a second control experiment was performed where Sn was not included in the flux. The voltage profile for Na removal from a flux with starting composition Na_6Si_2 is shown in Figure 2b. The initial drop in potential is from the cell not being at equilibrium (i.e., not fully relaxed) when the current pulse started, after which the OCP was close to 0 V vs Na/Na^+ , consistent with the high Na content in the flux. Oxidation resulted in a slightly sloped voltage profile at around 5 mV vs

 $\mathrm{Na/Na^+}$ until the flux composition was around $\mathrm{Na_{2.5}Si_2}$, after which the potential increased and a plateau at 58 mV was observed.

To understand the origins of the voltage profile features, the Na–Si and Na–Sn binary phase diagrams must be considered (Figure 3). According to the Gibbs phase rule, all intensive properties in a binary system, including the voltage, should vary continuously with composition within a single-phase region or remain invariant in a two-phase region. Figure 3a shows a portion of the Na–Sn phase diagram (adapted from ref 31) along with the OCP values from Figure 2a reproduced underneath at the appropriate compositions with connecting lines to guide the eye.

According to the Na-Sn binary phase diagram, the flux should remain molten at 485 °C until reaching a composition of ~43 atom % Sn. Therefore, a varying potential is expected when Na is removed from the flux in this region (i.e., singlephase process), as indicated by the gray line in the voltage profile in Figure 3a. At compositions between 43 and 50 atom % Sn, the phase diagram shows a two-phase region containing β -NaSn (melting point of 578 °C) and liquid phase (L); the voltage should remain constant in this composition region because all intensive properties are fully defined and there are no degrees of freedom remaining.³⁰ The experimental data in the lower part of Figure 3a show that the voltage vs composition behavior does not match those expected at this temperature. The most likely explanation is that the actual flux temperature is lower than expected. As seen in the Na-Sn phase diagram, the reaction temperature of 485 °C is just slightly higher than the melting temperature of Na₉Sn₄ and a number of two-phase regions containing solid and liquid phases. If there were poor thermal transport into the interior of the reactor, then it is possible that the actual flux temperature was lower than anticipated or measured with the thermocouple. For instance, the voltage plateau at ~40 mV seen when the flux composition is between ~25 and 40 atom % Sn suggests that the temperature may have been closer to 460 °C, which would put the reaction pathway within the two-phase region containing L + solid Na₉Sn₄. The 96 mV plateau is

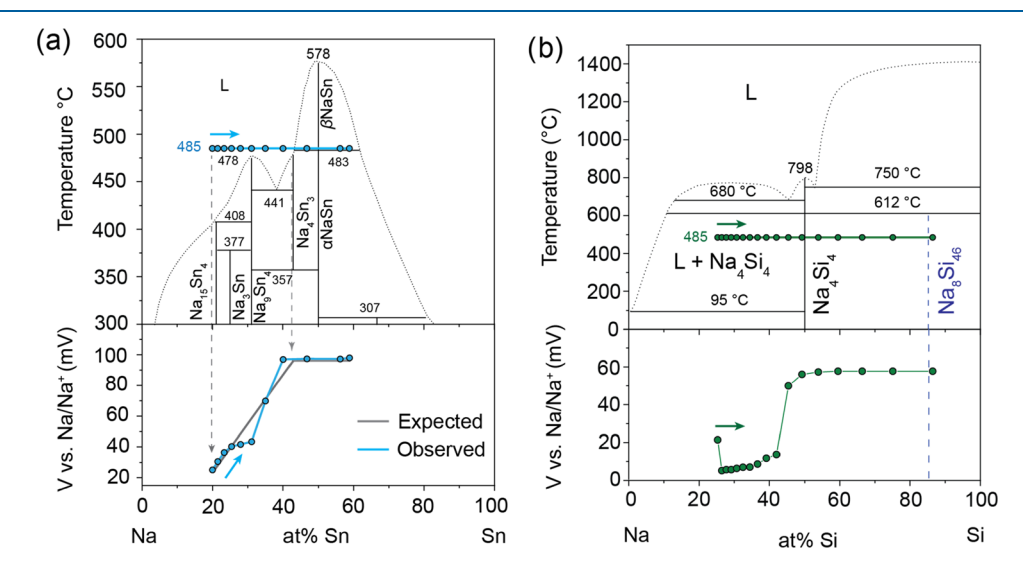


Figure 3. (a) Na–Sn phase diagram and OCP data observed from the measured GITT data shown in Figure 2a conducted at 485 $^{\circ}$ C from starting flux composition of Na₄Sn. (b) Na–Si phase diagram and OCP data measured from the GITT shown in Figure 2b conducted at 485 $^{\circ}$ C from starting flux composition of Na₆Si₂. The arrows indicate the direction of the desodiation process on the phase diagram.

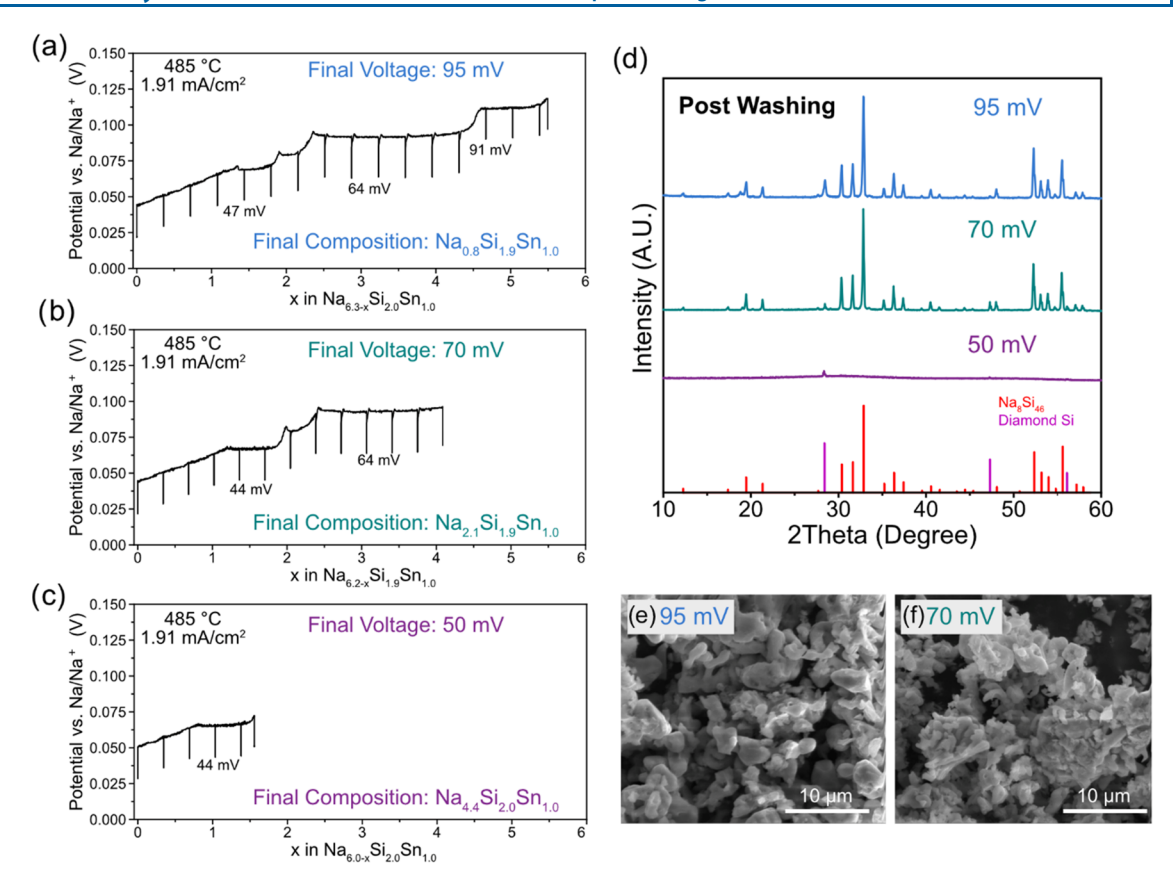


Figure 4. Galvanostatic intermittent titration technique (GITT) voltage profile at 485 °C (2 h current pulses at 1.91 mA/cm² separated by 10 min of relaxation at OCP) reaching a final OCP of (a) 95 mV, (b) 70 mV, and (c) 50 mV. (d) PXRD patterns of the products after the alcohol and acid wash. SEM micrographs of the washed products reaching a final relaxed voltage of (e) 95 mV and (f) 70 mV.

likely associated with the formation of a Na-Sn solid phase(s), but no attempts were made to isolate these and identify them.

On the other hand, the control experiment performed on Na₆Si₂ is consistent with the electrochemical characteristics expected for the Na-Si binary system (from ref 32). Two phases are initially present, Na and Na₄Si₄ (i.e., Na₆Si₂ can be considered as 4 Na + 2 NaSi, where Na₄Si₄ is also written as NaSi). Figure 3b shows that at 485 °C, the initial flux composition falls in the middle of the L + Na₄Si₄ region on the Na-Si phase diagram. Hence, the voltage is expected to remain constant during electrochemical oxidation because the amount of liquid phase will decrease until only Na₄Si₄ remains (i.e., two-phase process). This corresponds to the region from 0 < x < 3 in Na_{6-x}Si₂ in Figure 2b. After this point, the flux composition moves beyond 50 atom % Si into another twophase region. According to Morito et al., this two-phase region contains Na₄Si₄ and diamond cubic Si $(\alpha$ -Si),³² while others proposed that this region is divided into a two-phase region containing Na₄Si₄ and Na₈Si₄₆ (often referred to as Na₄Si₂₃) and then another one with Na₈Si₄₆ and α -Si.³³ The stoichiometry equivalent to Na₈Si₄₆ is indicated in the phase diagram in Figure 3b with a dotted blue line, showing that the synthesis removed enough Na from the flux to reach this composition. In our previous work, we found that Na₄Si₄ could be oxidized through a solid-state conversion reaction to form the type-I Na₈Si₄₆ clathrate at a voltage of 56 mV vs Na/Na⁺ (at 550 °C), 10 which is close to the voltage plateau observed here of 58 mV. PXRD analysis (Figure S3) of the products resulting from the electrochemical oxidation of Na₆Si₂ confirmed the formation of the type-I clathrate along with

some other phases, including Na_4Si_4 , suggesting that the precursor was not fully converted, which is reasonable considering the solid-state process.

Next, GITT of the flux containing Na:Si:Sn at a molar ratio of approximately 6:2:1 was performed. Figure 4a-c shows the voltage profiles obtained using a current density of 1.91 mA/ cm² at a temperature of 485 °C for different reaction times corresponding to final OCPs of 50, 70, and 95 mV vs Na/Na⁺. An example of the GITT profile as a function of time is presented in Figure S4. The final composition was calculated on the basis of the charge passed during the electrochemical reaction only (Supporting Information) and does not consider self-discharge from Na vapor reactions, which were described in our previous work 10 and will be discussed in more detail below. Briefly, the reaction of Na vapor (which is present in the reactor due to the high vapor pressure of sodium at these temperatures) with the products can result in re-formation of the Na₄Si₄ precursor. Therefore, the reported final composition is a lower bound and could possibly be higher if reaction of Na vapor with the product had occurred.

At the start of the reactions shown in Figure 4a–c, the voltage is around 24 mV Na/Na⁺, which is consistent with the presence of a liquid phase where Sn is dissolved in Na at the working electrode. Once the current is applied, there is a continuous increase in the potential as desodiation proceeds until reaching a plateau at 44–47 mV. The potential increases with further desodiation, and plateaus are observed at 64 mV and 91 mV. Notably, the voltage profile resembles the one for the control flux containing only Na and Sn (Figure 3a), but with the addition of the voltage plateau at 64 mV in between

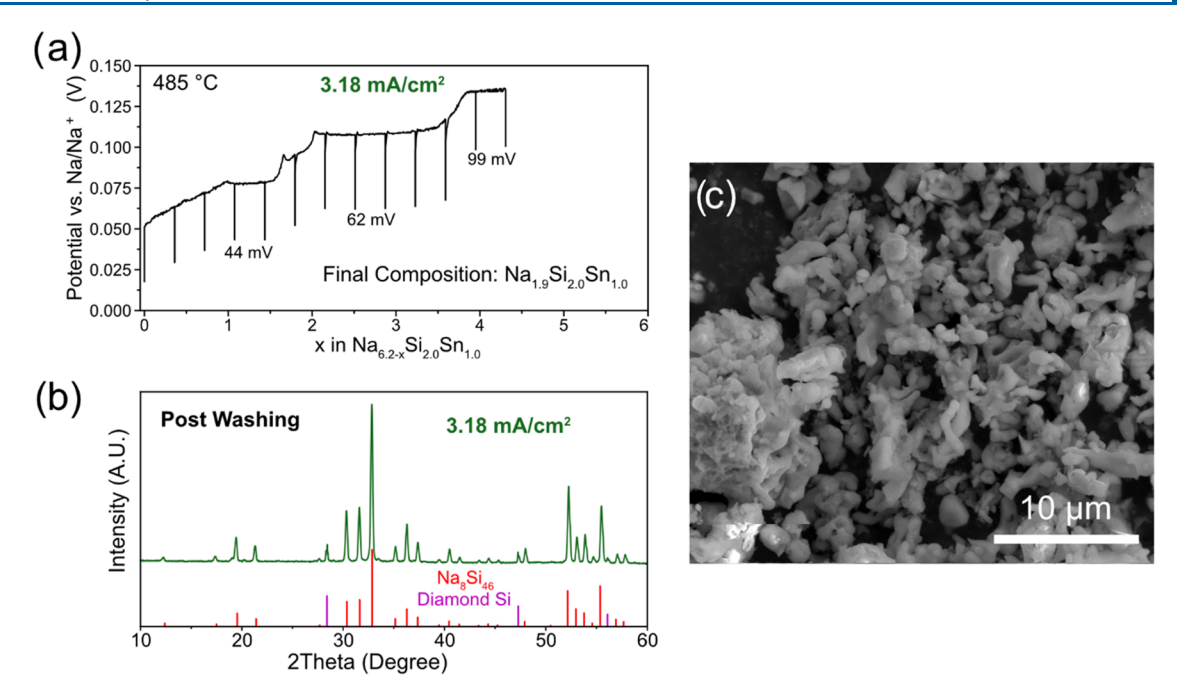


Figure 5. (a) Galvanostatic intermittent titration technique (GITT) voltage profile at 485 °C (1.2 h current pulses at 3.18 mA/cm² with 10 min of relaxation at OCP). (b) PXRD patterns of the products of the reaction after the alcohol and acid wash. (c) SEM micrographs of the reaction products obtained with a current of 3.18 mA/cm².

the plateaus at 47 and 91 mV (similar to those at 40 and 96 mV in the control flux); this implies that this feature at 64 mV is related to the nucleation and growth of the silicon clathrate phase.

The PXRD patterns of the products recovered after washing away the flux are shown in Figure 4d. For the sample that underwent the most desodiation (Figure 4a), the PXRD pattern shows reflections matching the type-I Na₈Si₄₆ clathrate phase along with minor impurities of α -Si and other unidentified phases. For the intermediate reaction (Figure 4b), the major product was also Na₈Si₄₆ with minor α -Si impurities. The PXRD pattern for the reaction reaching a final OCP of 50 mV, which stops before the voltage plateau at 64 mV is observed (Figure 4c), shows that the products are amorphous with a minor presence of α -Si. These results confirm that Na-Si clathrates can be synthesized by starting with a mixture of Na-Si-Sn flux and then driving the Na removal via electrochemical oxidation. Considering that the synthesized products are amorphous at low degrees of desodiation (i.e., before the observed voltage plateau at 64 mV), this also lends support to the process at 64 mV being related to the formation of the Na₈Si₄₆ clathrate phase.

SEM micrographs (Figure 4e,f) of the clathrate-containing products show that the resulting powder is composed of micron-sized particles with ligament-like morphology. The particle size appears to be larger for the reaction with a final OCP of 95 mV compared to 70 mV, possibly because of the longer time spent at the reaction temperature. Notably, this result is different from the previous reports preparing Na–Si clathrates from thermal evaporation out of a Na–Sn flux, where large single-crystal growth at temperatures from 450 to 550 °C was observed. The small particle sizes of our products obtained at 485 °C suggest the nucleation of many smaller Na–Si clathrate particles in this particular condition, precluding the growth of larger single crystals. The ligament-like morphology of the products is similar to our results from a

previous work, 10 where silicon clathrates were prepared electrochemically using solid-state oxidation, suggesting that the reactions might be going through a similar solid-state mechanism.

An important feature of using the electrochemical cell to mediate the synthetic process is the ability to directly control the current (and hence, reaction rate) independently of the temperature of the system. This is not possible for thermal evaporation approaches, as demonstrated by the work by Morito et al., which showed a clear dependence between the reaction rate and temperature. 18 To investigate the effect of the current density on the synthesis, the reaction with the Na-Si-Sn flux was performed at a higher current density of 3.18 mA/ cm². Figure 5 shows the GITT voltage profile along with the PXRD patterns and SEM micrograph of the obtained products after washing. The PXRD results show that the reaction with higher current density also resulted in the synthesis of Na₈Si₄₆ with minor α -Si impurities. From the SEM micrographs, the average particle size of the products synthesized at the higher current density is smaller than the product synthesized at 1.91 mA/cm². This is expected as a higher reaction rate reduces the time for coarsening of nuclei. Overall, these results show that by changing the current density of the reaction while keeping the temperature constant, different morphologies of clathrate particles can be grown. Such synthetic tunability can create more opportunities for understanding how the crystallite size of clathrates affects their properties.

The GITT profile carried out at 3.18 mA/cm² resembles the one at the lower current density (Figure 4a), with slight differences in the OCPs for the three voltage profiles. There are two notable differences. First, the voltage profile with the higher current density shows higher polarization (i.e., difference between the voltage under applied current and at OCP), which is consistent with the larger ohmic drop as more current is applied to the system. The higher overpotential required to achieve the higher current density should also increase the

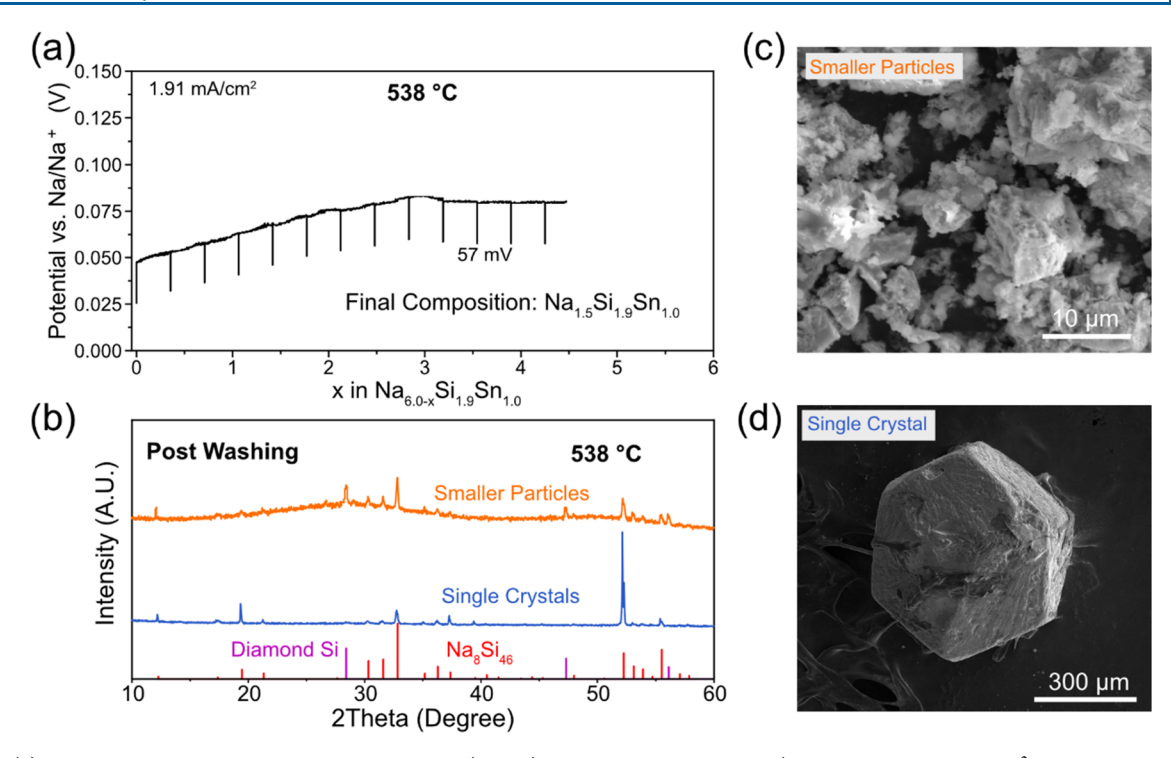


Figure 6. (a) Galvanostatic intermittent titration technique (GITT) voltage profile at 538 °C (2 h pulses at 1.91 mA/cm² with 10 min of relaxation at OCP). (b) PXRD patterns of the products after the alcohol and acid wash. SEM micrographs of the products obtained at 538 °C showing (c) smaller particles that were decanted during the washing procedure and (d) a Na_8Si_{46} single crystal.

number of nuclei that initially form, which leads to a larger number of small particles from which to grow.³⁴ Another difference is that the amount of capacity for each plateau or sloped region is lower at the higher current density. For instance, the highest voltage plateau of 99 mV (which is presumed to be the same process seen at 91 mV in Figure 4a) is reached upon removal of less Na from the flux than in the reaction carried out at a lower current density. This suggests that there was "less" Na₄Si₄ precursor present in the reaction compared to the one with a lower current density. However, both experiments had the same starting flux composition. This discrepancy can be readily explained by the aforementioned Na vapor self-discharge reaction, which drives the overall reaction backward to re-form Na₄Si₄, which can subsequently react again to form more of the clathrate product. The reaction carried out at higher current densities reaches completion faster due to the faster reaction rate. The system therefore spends less time at the elevated reaction temperature, meaning there is less time for the formed products to react with Na vapor and re-form Na₄Si₄ compared to the reaction at a lower current density. Future experiments will be required to quantify the Na self-discharge as its exact contributions are currently unknown. It is also possible to use a non-Na-metal electrode (e.g., Sn) to mitigate the Na vapor pressure as demonstrated earlier in our previous work, 10 but this complicates the interpretation of the cell voltage because the potential of the Sn electrode would also change over the course of the reaction as its composition changes.

In addition to changing the reaction rate, the temperature can be changed while keeping the current density constant to isolate the effects of temperature on the reaction. To demonstrate this, a reaction was conducted at 538 °C to evaluate the effect of temperature while using the same current density of 1.91 mA/cm². The GITT voltage profile of the

experiment (Figure 6a) shows that the higher temperature resulted in a large difference in the electrochemical behavior. At 538 °C, there is a continuously sloped region from the start of the reaction until reaching a voltage plateau at 57 mV. The continuous increase of potential suggests that the Na–Sn components are fully molten over this composition range, which is consistent with the phase diagram (Figure 3a). At 57 mV, a plateau is observed, which is attributed to the formation of the Na₈Si₄₆ clathrate phase on the basis of the similar voltage (56 mV) seen in our previous work using electrochemical solid-state desodiation of Na₄Si₄ at 550 °C to form Na₈Si₄₆. Notably absent is the voltage plateau at ~44 mV, which is attributed to the nucleation of solid Na–Sn phases at 485 °C (corresponding to the plateau at ~40 mV in Figure 2a).

As discussed previously, the products obtained at 485 °C consisted of small particles of the Na₈Si₄₆ clathrate phase (Figure 4f). In contrast, the products observed after the reaction at 538 °C were single crystals along with an amorphous phase composed of small particles. During the postsynthesis washing, the large crystals and smaller particles were separated by decanting the suspended particles, leaving behind the large single crystals. The PXRD pattern of a small amount of crushed single crystals (Figure 6b) shows different intensities of the reflections that do not match the PXRD pattern, suggesting that there are not enough crystallites to achieve the averaged PXRD intensity, which supports the single crystalline nature of the products. The suspended particles were mostly amorphous with small amounts of α -Si and Na₈Si₄₆. We speculate that the amorphous component is unreacted Na₄Si₄, suggesting that the conversion reaction to Na₈Si₄₆ did not go to completion. Figure 6c,d shows the SEM images of the smaller products and an \sim 600 μ m sized faceted crystal, respectively. EDS of the single crystal showed that the

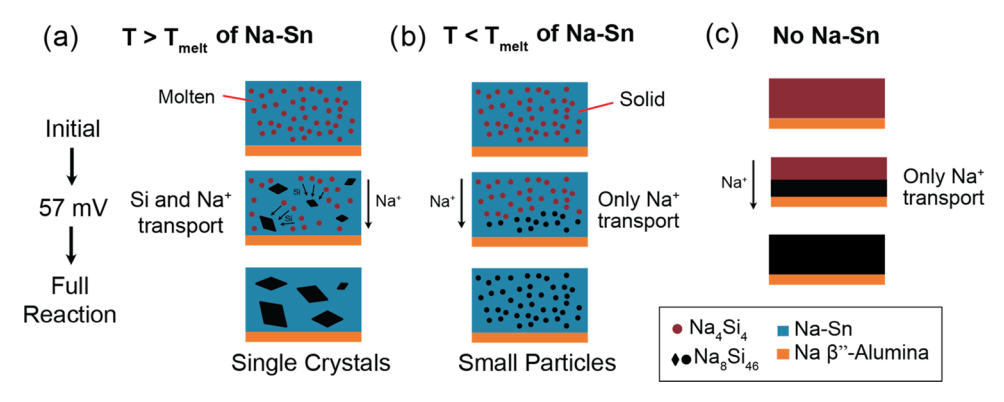


Figure 7. Scheme illustrating the different reaction mechanisms for electrochemical synthesis of Na_8Si_{46} clathrate from Na_4Si_4 . (a) When the reaction temperature is sufficiently high to melt Na-Sn, the Na-Sn phase enables mass transfer of Na^+ and Si atoms in the flux, which allows for the coarsening and growth of large single crystals of clathrate. (b) When the temperature is below the melting point of Na-Sn, the Na-Sn is solid and only mediates the mass transfer of Na^+ ions to the solid electrolyte, which results in the formation of small particles of the type-I clathrate phase. (c) In the absence of Na-Sn mediator completely, Na^+ removal from Na_4Si_4 results in the formation of the clathrate phase at the interface with the solid electrolyte; the formed Na_8Si_{46} products then mediate the Na^+ transport as the two-phase boundary moves further away from the electrolyte.

composition is consistent with that of a Na-filled Si clathrate with the composition of ca. $Na_{7.6}Si_{46.4}$ (Figure S5). SCXRD of the products confirmed that the large crystals are the type-I phase with a lattice parameter of 10.1852(18) Å and a refined composition of Na_8Si_{46} (Table S1-S2). The morphology of the single crystals is similar to that reported by Morito et al. for the type-I clathrate phase made by conventional flux methods, ^{16,18} suggesting that a similar growth mechanism is achieved via the electrochemical desodiation of the Na-Si-Sn flux.

On the basis of these results, the role of the Sn component in the flux during the electrochemical reaction becomes clear. If Sn is absent from the reaction (i.e., as in the control reaction in Figures 2b and 3b), the liquid Na metal is removed from the working electrode compartment prior to the nucleation of the type-I Na₈Si₄₆ phase. This is because the oxidation potential of the Na metal (0 V vs Na/Na⁺) is lower than the potential at which the clathrate begins to form (around 62-64 mV vs Na/ Na⁺ at 485 °C or 56 mV vs Na/Na⁺ at 538 °C). Once all of the Na is removed, there is no more liquid phase to promote Si mass transport, resulting in a solid-state conversion reaction between Na₄Si₄ and Na₈Si₄₆. When Sn is present in the flux, the Na remains dissolved in the Na-Sn solution over a wider range of potentials (from 25 to ~90 mV vs Na/Na⁺) except for when Na₄Sn₉ solid forms at around 44-47 mV. Notably, the potential corresponding to the formation of Na₈Si₄₆ falls in between the two voltage plateaus associated with the formation of solid Na-Sn phases (at 47 and 91 mV, Figure 4a), meaning that Na-Sn is still present during the nucleation of Na₈Si₄₆. This is important as the Na-Sn component can thus act as a mass transport mediator during the nucleation and growth process of the Na₈Si₄₆ clathrate.

The observation that single-crystal growth was achieved at 538 °C and not 485 °C is good evidence that the Na–Sn component was not fully molten over the full composition range in the latter case. This point is illustrated in Figure 7, which shows a schematic of the proposed reaction mechanisms. Initially, the Na₄Si₄ precursor is surrounded by the Na–Sn phase, which will remain solid or become molten depending on the reaction temperature. If the temperature is higher than the melting point ($T_{\rm melt}$) of the Na–Sn phase, it is possible for Na₄Si₄ to dissolve in the flux and contribute to coarsening of the clathrate nuclei to form large single crystals, as was

observed at 538 °C (Figure 7a). On the other hand, if the temperature is lower than T_{melt} and solid Na-Sn is present, it will be more difficult for solid-state Si diffusion and likely only Na⁺ ions can be transported via the Na-Sn phase to the solid electrolyte (Figure 7b). This results in a local conversion of the Na₄Si₄ precursor to the clathrate phase near the interface with the solid electrolyte, which restricts particle growth and thus results in the small particles seen in all reactions performed at 485 °C. In the absence of the Na-Sn mediating phase, all of the Na+ removal from the Na₄Si₄ precursor must first take place via solid-state diffusion through a planar interface with the Na β'' -alumina solid electrolyte (Figure 7c). After product formation, continued desodiation of Na₄Si₄ must rely on Na⁺ transport through the formed clathrate phase. The high Na+ migration barriers³⁶ and porous nature of the formed clathrate products could explain why this process was associated with high polarization as seen in our previous work describing the solid-state electrochemical conversion of Zintl phase precursors to clathrates without a Na-Sn mediator. 10

The observation that the morphology and size of the clathrate crystals depend on whether Si mass transfer in the Na–Sn phase is possible at a given reaction temperature is consistent with results in conventional clathrate syntheses as well. For example, oxidation of Na₄Si₄ under vacuum results in polycrystalline powders while oxidation under applied pressure 14,15 or in a Na–Sn flux results in single crystals. 16,18 Due to the volume contraction between Na₄Si₄ and Na–Si clathrates, a mechanism enabling Si mass transport is required to form large single crystals or else the resulting structure is porous and polycrystalline. This is evident from the SEM and transmission electron microscopy (TEM) analysis of the Si clathrates synthesized via the thermal decomposition and electrochemical oxidation of Na₄Si₄ described in our previous work. 9,10

The ability to "switch" Si mass transport on and off via the melting temperature of the flux has interesting implications for the synthesis of clathrates for different applications. For instance, in Li-ion battery applications, generally small particles (micron-sized) are used to create composite electrodes with high surface area. In this view, the solid Na—Sn phase that blocks Si mass transport is an interesting synthetic pathway because it enables formation of smaller particles. In the case of

electronic and photovoltaic applications, large single-crystal substrates are often used, which means that the molten Na—Sn mediator with the ability to transport Si is of more interest.

Compared to the electrochemical synthesis method described in our previous work, 10,23 which used a solid-state conversion reaction between the Zintl phase precursor and clathrate (depicted in Figure 7c), the approach using the Na-Sn mass transport mediator has several advantages. First, the reactions using the mediator displayed constant polarization that remained low over the whole course of the reactions. In our previous work, the polarizations increased dramatically over the course of the reaction. 10,23 Low polarizations are favorable because of the ability to access high current densities (i.e., reaction rates), which could accelerate the synthesis process and result in different product morphologies. The low polarization observed (26 mV at 1.91 mA/cm²) even when the Na-Sn mediator was solid is attributed to the fast solid-state Na⁺ diffusion in Na-Sn phases, which is evidenced by the ability of Sn to be used as room-temperature electrode for Naion batteries.³⁷ Second, the method demonstrated herein is easier to scale than the solid-state method because there are fewer mass transport limitations as Na diffusion does not have to occur through the interface between a pellet of the Zintl phase precursor and the solid electrolyte (Figure 7c), but rather through a Na-ion conducting medium in which the Zintl phase is well dispersed.

Overall, the electrochemical approach with assistance from a Na–Sn mass transport mediator shows promise as a flexible synthetic method for Si clathrates. The elucidation of the reaction mechanisms can be easily transferred to other reactive Zintl phase precursors and other mass transport mediators. The work presented here also demonstrates how the flux-based electrochemical method can be used to develop a better understanding of the chemistry occurring during the reaction as information is being collected in situ via the voltage profile characteristics. This could lead to a more rational design of mass transport mediators (e.g. fluxes) and reaction conditions.

4. CONCLUSIONS

A flux-based electrochemical synthetic approach using a twoelectrode cell with a geometry analogous to that of a Na-S battery was demonstrated for preparing type-I Na_8Si_{46} clathrate crystals. The working electrode comprised a mixture of Na-Si-Sn in a 6:2:1 molar ratio, and the counter/reference electrode was Na metal. Anodic current was applied to the working electrode to drive the formation of Na₈Si₄₆. The voltage profile of the desodiation reaction was analyzed, and a voltage plateau at 64 mV at 485 °C was confirmed to correspond to the nucleation and growth of the Na₈Si₄₆ phase. The effect of current density (reaction rate) and temperature on the reaction products was investigated. Using a temperature of 538 °C resulted in the growth of large single crystals (~600 μ m) of Na₈Si₄₆ in contrast to the smaller particles grown at 485 °C. This difference is attributed to the fully liquid nature of the Na-Sn component at 538 °C during the reaction, which is important for single-crystal growth by mediating the diffusion of Si. Overall, the electrochemical method is a promising method of growing Si clathrates or other intermetallic structures and provides in situ information about the potential of the system, which can be useful for developing a deeper understanding of the chemistry that is taking place.

ASSOCIATED CONTENT

Supporting Information

The Supporting Information is available free of charge at https://pubs.acs.org/doi/10.1021/acs.inorgchem.2c03811.

Detailed experimental procedures for the preparation of Zintl phase precursor, electrochemical reactor assembly, electrochemical measurements, postsynthesis washing procedure, materials characterization, summary of the crystallographic data obtained from the single-crystal X-ray diffraction measurements, photographs of the reactor assembly, PXRD patterns of the as-synthesized Na₄Si₄ precursor and products from electrochemical oxidation of Na₆Si₂, GITT voltage profile as a function of time, and EDS spectrum of Na₈Si₄₆ single crystal (PDF)

Accession Codes

CCDC 2213062 contains the supplementary crystallographic data for this paper. These data can be obtained free of charge via www.ccdc.cam.ac.uk/data_request/cif, or by emailing data_request@ccdc.cam.ac.uk, or by contacting The Cambridge Crystallographic Data Centre, 12 Union Road, Cambridge CB2 1EZ, UK; fax: +44 1223 336033.

AUTHOR INFORMATION

Corresponding Author

Candace K. Chan — Materials Science and Engineering, School for Engineering of Matter, Transport and Energy, Arizona State University, Tempe, Arizona 85827, United States;
ocid.org/0000-0003-4329-4865; Phone: (480) 727–8614; Email: candace.chan@asu.edu

Authors

Andrew Dopilka — Materials Science and Engineering, School for Engineering of Matter, Transport and Energy, Arizona State University, Tempe, Arizona 85827, United States;
occid.org/0000-0003-3474-2187

Svilen Bobev — Department of Chemistry and Biochemistry, University of Delaware, Newark, Delaware 19716, United States; © orcid.org/0000-0002-0780-4787

Complete contact information is available at: https://pubs.acs.org/10.1021/acs.inorgchem.2c03811

Author Contributions

The manuscript was written through contributions of all authors. A.D. designed the electrochemical reactor and performed electrochemical measurements, materials characterization, and data analysis. A.D. and S.B. prepared the Zintl phase compounds. S.B. performed the structure analysis. C.K.C. assisted with the electrochemical analysis. All authors have given approval to the final version of the manuscript.

Notes

The authors declare no competing financial interest.

ACKNOWLEDGMENTS

This work was supported by funding from NSF from the awards DMR-2004514 and DMR-2004579. A.D. acknowledges support from ASU Fulton Schools of Engineering Dean's Fellowships. The authors acknowledge the use of facilities within the Eyring Materials Center (supported in part by NNCI-ECCS-1542160) and the Instrument Design and Fabrication Core Facility at Arizona State University.

REFERENCES

- (1) Nolas, G. S.; Beekman, M.; Gryko, J.; Lamberton, G. A.; Tritt, T. M.; McMillan, P. F. Thermal Conductivity of Elemental Crystalline Silicon Clathrate Si₁₃₆. *Appl. Phys. Lett.* **2003**, *82*, 910–912.
- (2) Gryko, J.; McMillan, P. F.; Marzke, R. F.; Ramachandran, G. K.; Patton, D.; Deb, S. K.; Sankey, O. F. Low-Density Framework Form of Crystalline Silicon with a Wide Optical Band Gap. *Phys. Rev. B Condens. Matter Mater. Phys.* **2000**, *62*, R7707–R7710.
- (3) Martinez, A. D.; Krishna, L.; Baranowski, L. L.; Lusk, M. T.; Toberer, E. S.; Tamboli, A. C. Synthesis of Group IV Clathrates for Photovoltaics. *IEEE J. Photovoltaics* **2013**, *3*, 1305–1310.
- (4) Kume, T.; Ohashi, F.; Nonomura, S. Group IV Clathrates for Photovoltaic Applications. *Jpn. J. Appl. Phys.* **2017**, *56*, No. 05DA05.
- (5) Fix, T.; Vollondat, R.; Ameur, A.; Roques, S.; Rehspringer, J. L.; Chevalier, C.; Muller, D.; Slaoui, A. Silicon Clathrate Films for Photovoltaic Applications. *J. Phys. Chem. C* **2020**, *124*, 14972–14977.
- (6) Moriguchi, K.; Munetoh, S.; Shintani, A. First-Principles Study of Si_{34-x}Ge_x Clathrates: Direct Wide-Gap Semiconductors in Si-Ge Alloys. *Phys. Rev. B* **2000**, *62*, 7138–7143.
- (7) Langer, T.; Dupke, S.; Trill, H.; Passerini, S.; Eckert, H.; Pöttgen, R.; Winter, M. Electrochemical Lithiation of Silicon Clathrate-II. *J. Electrochem. Soc.* **2012**, *159*, A1318–A1322.
- (8) Wagner, N. A.; Raghavan, R.; Zhao, R.; Wei, Q.; Peng, X.; Chan, C. K. Electrochemical Cycling of Sodium-Filled Silicon Clathrate. *ChemElectroChem* **2014**, *1*, 347–353.
- (9) Dopilka, A.; Weller, J. M.; Ovchinnikov, A.; Childs, A.; Bobev, S.; Peng, X.; Chan, C. K. Structural Origin of Reversible Li Insertion in Guest-Free, Type-II Silicon Clathrates. *Adv. Energy Sustainability Res.* **2021**, *2*, No. 2000114.
- (10) Dopilka, A.; Childs, A.; Bobev, S.; Chan, C. K. Solid-State Electrochemical Synthesis of Silicon Clathrates Using a Sodium-Sulfur Battery Inspired Approach. *J. Electrochem. Soc.* **2021**, *168*, No. 020516.
- (11) Kasper, J. S.; Hagenmuller, P.; Pouchard, M.; Cros, C. Clathrate Structure of Silicon Na_8Si_{46} and Na_xSi_{136} (x <11). Science 1965, 150, 1713–1714.
- (12) Reny, E.; Gravereau, P.; Cros, C.; Pouchard, M. Structural Characterisations of the Na_xSi₁₃₆ and Na₈Si₄₆ Silicon Clathrates Using the Rietveld Method. *J. Mater. Chem.* **1998**, *8*, 2839–2844.
- (13) Ramachandran, G. K.; Dong, J.; Diefenbacher, J.; Gryko, J.; Marzke, R. F.; Sankey, O. F.; McMillan, P. F. Synthesis and X-Ray Characterization of Silicon Clathrates. *J. Solid State Chem.* **1999**, *145*, 716–730.
- (14) Beekman, M.; Baitinger, M.; Borrmann, H.; Schnelle, W.; Meier, K.; Nolas, G. S.; Grin, Y. Preparation and Crystal Growth of Na₂₄Si₁₃₆. *J. Am. Chem. Soc.* **2009**, *131*, 9642–9643.
- (15) Stefanoski, S.; Beekman, M.; Wong-Ng, W.; Zavalij, P.; Nolas, G. S. Simple Approach for Selective Crystal Growth of Intermetallic Clathrates. *Chem. Mater.* **2011**, 23, 1491–1495.
- (16) Morito, H.; Shimoda, M.; Yamane, H. Single Crystal Growth of Type I Na–Si Clathrate by Using Na–Sn Flux. *J. Cryst. Growth* **2016**, 450, 164–167.
- (17) Krishna, L.; Baranowski, L. L.; Martinez, A. D.; Koh, C. A.; Taylor, P. C.; Tamboli, A. C.; Toberer, E. S. Efficient Route to Phase Selective Synthesis of Type II Silicon Clathrates with Low Sodium Occupancy. *CrystEngComm* **2014**, *16*, 3940–3949.
- (18) Morito, H.; Shimoda, M.; Yamane, H.; Fujiwara, K. Crystal Growth Conditions of Types I and II Na-Si Clathrates by Evaporation of Na from a Na-Si-Sn Solution. *Cryst. Growth Des.* **2018**, *18*, 351–355.
- (19) Böhme, B.; Guloy, A.; Tang, Z.; Schnelle, W.; Burkhardt, U.; Baitinger, M.; Grin, Y. Oxidation of M_4Si_4 (M = Na, K) to Clathrates by HCl or H_2O . *J. Am. Chem. Soc.* **2007**, *129*, 5348–5349.
- (20) Beekman, M.; Nenghabi, E. N.; Biswas, K.; Myles, C. W.; Baitinger, M.; Grin, Y.; Nolas, G. S. Framework Contraction in Na-Stuffed Si(cF136). *Inorg. Chem.* **2010**, *49*, 5338–5340.
- (21) Blosser, M. C.; Nolas, G. S. Synthesis of Na₈Si₄₆ and Na₂₄Si₁₃₆ by Oxidation of Na₄Si₄ from Ionic Liquid Decomposition. *Mater. Lett.* **2013**, *99*, 161–163.

- (22) Böhme, B. An Electrochemical Approach toward the Metastable Type II Clathrate Germanium Allotrope. *Inorg. Chem.* **2020**, *59*, 11920–11924.
- (23) Dopilka, A.; Ovchinnikov, A.; Childs, A.; Bobev, S.; Peng, X.; Chan, C. K. Synthesis of Type II Ge and Ge-Si Alloyed Clathrates Using Solid-State Electrochemical Oxidation of Zintl Phase Precursors. *Inorg. Chem.* **2022**, *61*, 12363–12372.
- (24) Morito, H.; Yamane, H.; Umetsu, R. Y.; Fujiwara, K. Seeded Growth of Type-II Na₂₄Si₁₃₆ Clathrate Single Crystals. *Crystals* **2021**, *11*, 808.
- (25) Urushiyama, H.; Morito, H.; Yamane, H.; Terauchi, M. Na-Ga-Si Type-I Clathrate Single Crystals Grown via Na Evaporation Using Na-Ga and Na-Ga-Sn Fluxes. *RSC Adv.* **2018**, *8*, 40505–40510.
- (26) Urushiyama, H.; Morito, H.; Yamane, H. Single Crystal Growth and Structure Analysis of Type-I (Na/Sr)-(Ga/Si) Quaternary Clathrates. *RSC Adv.* **2019**, *9*, 14586–14591.
- (27) Hueso, K. B.; Armand, M.; Rojo, T. High Temperature Sodium Batteries: Status, Challenges and Future Trends. *Energy Environ. Sci.* **2013**, *6*, 734–749.
- (28) Weppner, W.; Huggins, R. A. Determination of the Kinetic Parameters of Mixed-Conducting Electrodes and Application to the System Li₃Sb. *J. Electrochem. Soc.* **1977**, *124*, 1569.
- (29) Tamaki, S.; Ishigurot, T.; Takedag, S. Thermodynamic Properties of Liquid Na-Sn Alloys. *J. Phys. F: Met. Phys.* **1982**, *12*, 1613–1637.
- (30) Huggins, R. A. Advanced Batteries: Materials Science Aspects; Springer Science & Business Media: New York, 2008.
- (31) Ellis, L. D.; Hatchard, T. D.; Obrovac, M. N. Reversible Insertion of Sodium in Tin. *J. Electrochem. Soc.* **2012**, *159*, A1801–A1805.
- (32) Morito, H.; Yamada, T.; Ikeda, T.; Yamane, H. Na-Si Binary Phase Diagram and Solution Growth of Silicon Crystals. *J. Alloys Compd.* **2009**, 480, 723–726.
- (33) Mali, A.; Petric, A. EMF Measurements of the Na-Si System. *J. Phase Equilib. Diffus.* **2013**, 34, 453–458.
- (34) Gunawardena, G.; Hills, G.; Montenegro, I.; Scharifker, B. Electrochemical Nucleation. Part I. General Considerations. *J. Electroanal. Chem.* **1982**, 138, 225–239.
- (35) Sangster, J.; Bale, C. W. The Na-Sn (Sodium-Tin) System. *J. Phase Equilib.* **1998**, *19*, 76–81.
- (36) Dopilka, A.; Peng, X.; Chan, C. K. Ab Initio Investigation of Li and Na Migration in Guest-Free, Type I Clathrates. *J. Phys. Chem. C* **2019**, 123, 22812–22822.
- (37) Stratford, J. M.; Mayo, M.; Allan, P. K.; Pecher, O.; Borkiewicz, O. J.; Wiaderek, K. M.; Chapman, K. W.; Pickard, C. J.; Morris, A. J.; Grey, C. P. Investigating Sodium Storage Mechanisms in Tin Anodes: A Combined Pair Distribution Function Analysis, Density Functional Theory, and Solid-State NMR Approach. *J. Am. Chem. Soc.* **2017**, *139*, 7273–7286.